Indentation hardness and scratch tests for thin layers manufactured by sol-gel process

Hervé Piombini, Christel Ambard, François Compoint, Karine Valle, Philippe Belleville, Clément Sanchez

Indentation hardness and scratch tests for thin layers manufactured by sol-gel process

A. GUEDICHE,[1,*] F. COMPOINT,[1] C. BOSCHER,[1] C. STELIAN,[2] AND H. PIOMBINI[1,*]

[1] *CEA, DAM Le Ripault, F-37260 Monts,*
[2] *Laboratoire Université Grenoble Alpes, CNRS, Grenoble INP, SIMAP, F-38000, Saint Martin d'Hères, France*
amira.guediche@cea.fr, herve.piombini@cea.fr

Abstract: Indentation hardness and scratch tests are common techniques used in industries and laboratories to determine the mechanical properties of thin films. Here, we propose to determine a relative value of the elastic modulus and hardness of thin films composed of a mixture of polydimethylsiloxane and polymeric silica with elastic properties and self-healing effects. For this study, a homemade nano-indenter and nano scratch tester has been designed with a microscope and a scanning stage allowing the carrying out of measurements on transparent materials having a weak elastic modulus and the possibility to identify a self-healing effect of these films.

Keywords: nano-indentation, nano-indenter, thin film, PDMS, polymeric silica, elastic modulus, hardness, nano scratch test, self-healing.

1. Introduction

Indentation and scratch tests are used in laboratories and industries to determine the mechanical properties of thin films and adhesion. Generally, a diamond indenter with a specific geometry (spherical, pyramidal or conical) is

used to impress its shape on the film surface by using a known load [1-2]. However, the measured hardness differs as a function of the indenter shape (Brinell, Vickers, Rockwell, Shore… hardness) and associated parameters (duration, load…). The typical problems encountered with the indentation in the field of thin films are linked to their weak thickness and more particularly, for the sol-gel films, to their high porosity. The aim is to study films with elastic properties that could absorb shocks induced by the power laser beam absorption. Indeed, these shockwaves can increase the size of previously produced laser damage [3]. The absorption processes due to laser beams by a thin film are numerous and complex. The aim of this paper is limited to having better knowledge of the mechanical properties of elastic layers to improve studies on laser-matter interaction with elastic layers. As such, the effects of the power laser beam absorption on the layers are not developed in this paper. This study is part of the LMJ (Laser MégaJoule) project. It is a key component of the simulation program of the Commissariat aux Energies Atomiques et aux énergies renouvelables. Its purpose is to study, on a very small scale, the behavior of materials under extreme conditions like those reached during the operation of nuclear weapons. The LMJ officially became operational in October 2014, with the weapon physics experiments. It was designed to achieve inertial confinement fusion. It will deliver in a few billionths of a second more than one million joules of light energy on a target measuring a few millimeters in diameter. The optical components of laser

channels working in transmission are produced by a sol-gel process on which laser-damage appears from time to time. We hope that the introduction of an elastic layer will help reduce the amplitude of the mechanical waves generated by the weak absorption of the laser pulse and so decrease the risk of further laser damage (**Fig. 1**). Indeed, as the propagation of shock waves depends on the material elastic modulus E (the sound velocity C_{sound} is equal to $\sqrt{E/\rho}$ with ρ the density), one way to control it is by developing layers with weak elastic modulus to cover the optical components made of fused silica ($C_{sound} \approx 5$ km.s^{-1} [4-5] in fused silica while $C_{sound} \approx 1.7$ km.s^{-1} in our sol-gel films [6]).

The layers studied here can also have self-healing properties to heal the potential damage that could appear under laser flux [7-10] as shown in section 3.3. They are composed of cocondensation between polydimethylsiloxane (PDMS, formula $HO[Si(CH_3)_2O]_nH$) [11-12] and tetraethylorthosilicate [11, 13-16]. The resulting nanocomposites demonstrate tunable elastic properties and a possible self-healing effect thanks to the incorporation of PDMS into the SiO_2 network. To optimize these films, we have used various techniques to identify the optical characteristics [17-20], measure their stress level [21] and determine their elastic modulus [5-6, 22]. In this paper, we used a homemade nano-indenter built from a microscope equipped with an x*y motorized stage. It makes measurements on transparent elastic materials with weak elastic moduli that are deposited upon a substrate as thin film. The

possible self-healing effect of our transparent materials is also checked. In the future, we wish to increase the laser damage threshold of our components by reducing mechanical shock waves thanks to a viscoelastic layer (**Fig. 1**).

2. Experimental setup and characterization

2.1 Experimental setup and calibration

Hardness measurements were carried out with a laboratory-built nano-indenter/scratch tester that can be modified based on experimental needs. Nano scratch test measurements were performed with various associated parameters [23-25]. The experimental setup is given in **Fig. 2**.

This laboratory-built indenter was designed with a Leica DMR microscope equipped with x&y scanning stages (Multicontrol 2000) with a range of 47.3*74.4 mm² and a 1 µm resolution, a V500 digital camera with a 640x480 pixel chip for imprint observation [26], a conical diamond indenter (**Fig. 3**), a microscope with objectives ranging from X5 to X100, operable in brightfield (BF), darkfield (DF) and differential interference contrast (DIC). This equipment was computer-driven by a LabVIEW program that controlled microscope focusing. Z-axis resolution was 50 nm. The setting and acquisition of camera settings used (gamma, gain, shutter…), the scanning stage movements (acceleration, speed, courses along x and y) and the necessary corrections of slope and concentricity defects caused by objectives used were monitored by the computer. The sample illumination was defined

by the integration of the luminous flux reflected by a reference sample (polished silica substrate). To ensure the measurement reproducibility, this light intensity adjustment was better by 1 % compared to our reference intensity.

The indenter and its holder were fixed on a rail (**Fig. 2**) positioned above a scanning stage that held the tested sample. The conical diamond indenter had a 61.3° angle and seemed satisfactory when observed through an optical microscope (**Fig. 3**).

Scanning Electron Microscope (SEM) photography showed that the indenter is more spherical than conical (**Fig. 4**) for our application, with a tip radius estimated at 20 µm. In section 2.3 further details will be developed about the indenter shape to consider.

Motorized stages enabled the adjustment of the indenter location along the y-axis. The z-axis was fitted with the microscope to see the mark left by the indenter in the camera field. Correction of the slope coming from either the parallelism defects of the substrate or the stage displacement can be done thanks to the previous acquisition of some images' heights located at three extreme spots of the measurement surface (nevertheless the samples, being optically polished, should be flat). This correction was done during the indenter displacement by adjusting the z-position. The z-position at which focalization was satisfactory was determined using a reference image on which the focalization had been correctly adjusted. Before each measurement,

an initial set of images corresponding to future locations of either the imprints or the scratches were displayed and stored to consider possible local defects of the analyzed layer. After indentation tests, images showing the change of either the indentation matrix or the scratch state were recorded to follow their evolution and determine the appropriate self-repairing kinetic. Microscope focus was adjusted with the vertical displacement of its stage, enabling control over the load applied on the sample. The indentation or scratch force was calibrated thanks to an accurate weighing scale (accuracy = 0.1 mg). This calibration method only gives a relative value of the load. Indeed, the scale can be modeled as a spring and the indentation or scratch force, when applied on the surface of the scale, gives a result of the load applied relative to the stiffness of the scale and of the layer. This explains why a β coefficient is used for the F load applied. The indenter was attached to the motorized translation stage with a 0.1 µm resolution. Indenter placement was adjusted to be in contact with the weighing scale tray. The weight was then recorded according to displacement. The curve is given in **Fig. 5** with a slope of 0.324 $mN.\mu m^{-1}$. As the microscope sensitivity along the z-axis was equal to z = 50 nm for its displacement, the load sensitivity was equal to 1.65 mg, so approximatively 16 µN. For more details on illustrations and calibration of the system, please refer to reference [6].

Fig. 6 and **Fig. 7** respectively describe our device operating mode for the indentation and the scratch. A matrix of $N_x \times Ny$ points with a S_x step in x and

a S_y step in y has been carried out to test hardness. Between each point, the indenter depth increased by Δz (µm). Load was thus increased by 0.32 $\beta.\Delta z$ (mN) and the slopes relative to the sample flatness and the orientation defects of the microscope stages were corrected. The images corresponding to each indentation location were then stored with a suitable objective microscope. The indentation duration, although adjustable, remained constant when the indentation matrix was carried out. It was fixed to 1 second. It was possible to set the speed of penetration between 1 and 20 $mm.s^{-1}$, but 20 $mm.s^{-1}$ was selected for our tests. As the viscoelastic response of the layer studied here took a few hours, a time delay of a few seconds between indentation and image recording does not therefore lead to a measurement bias. For the scratch test, N_x lines with a S_x step in x have been carried out. During the displacement, the slope related to the sample flatness or the orientation defect of the microscope stages has also been corrected. Pictures were taken before and after the scratch test with the appropriate objective microscope.

Fig. 8 is an example of two intercrossed indentation matrices with a step of 0.25 mm and a vertical motion of ΔZ = 200 or 800 nm between each line. Moreover, according to the indentation images taken, it has been possible to determine the aspect of a satisfactory indentation.

2.2 Evaluation of contact stiffness

In the context of a typical indentation, indenter resistance to elastic and plastic deformation is much greater than that of the surface layer. A schematic diagram of the indenter is shown in **Fig. 9**.

The indenter can be described as a column with an extremity composed of a linear-elastic element with a given spring stiffness. The stiffness of the k indentation system after contact with the surface layer is related to the spring and contact stiffness (the elements are in series):

$$\frac{1}{k} = \frac{1}{k_s} + \frac{1}{k_t} \tag{1}$$

The stiffness k_s of the spring is given by:

$$k_s = \frac{E_s \,.\, A_s}{L_s} \tag{2}$$

With E_s the elastic modulus of the indenter column, A_S the cross-sectional surface and L_s the length of the column (L_s = b - a). This latter is made of steel, so E_s = 200 GPa [27], and knowing the column to be a 5 mm circular rod of diameter 1.07 mm we find $k_s \approx 36.10^6$ N.m^{-1}.

The contact stiffness k_t is given by [27] (for a circular contact): k_t = 2.r.M, where M is the indentation modulus of tip-surface. It considers deformation in both the tip and the surface during contact and is equal to:

$$\frac{1}{M} = \frac{1}{M_{tip}} + \frac{1}{M_{\text{Surface layer}}} \tag{3}$$

With M_{tip} the indentation modulus of the tip and $M_{Surface\ layer}$ the indentation modulus of the layer. Supposing the material to be elastically isotropic, we obtain the following relation:

$$M_{Surface\ layer}=\frac{E_{sl}}{1-\nu_{sl}^2} \quad (4)$$

Here, the layer considered is a hybrid silica-PDMS with an E_{sl} elastic modulus and ν_{sl} Poisson's ratio. As E_{sl} = 50 GPa (if we take the higher value - obtained with 10 wt. % of PDMS [22]) and $\nu_{sl} = 0.5$, it gives $M_{Surface\ layer} \approx 67$ GPa. Moreover, for a typical diamond indenter used in nano-indentation [27], M_{tip} = 1,150 GPa. Thus, the indentation modulus is M ≈ 63 GPa. Then, the contact stiffness, for a nano-indentation contact radius of r = 20 µm is $k_t \approx 2.5$ MN.m^{-1}. The contact stiffness is less than the spring stiffness $k_t < k_s$, so most of the indenter displacement is taken up by the contact and we have negligible deformation of the spring (a << b). Additionally, the value of the surface indentation modulus is less than the indenter modulus: $M_{Surface\ layer} < M_{Tip}$. This explains why it is reasonable to neglect the indenter column stiffness. However, it is planned to properly determinate its value in further experiments.

2.3 Determination of the contact area

The experimental scratch test is given in **Fig. 10**. It makes scratches, i.e. lateral displacement of the tip with a controlled depth on the layer surface in

order to penetrate the thin film and inflict damage on the scale of its thickness. The scratches have a maximum target depth of half the film thickness.

Each image (**Fig. 11. a**) of the imprint taken either in brightfield, darkfield or in differential interference contrast (DIC) was treated (**Fig. 11. b**) with the ImageJ software [28] to measure the contact surface $A_{imprint}$, also called projected area or surface. A portion of the image presenting the indentation was selected. Then, an analysis of particles was applied to the selected portion of the image. The indentation surface was given by the main surface defect. The pixel sizes of the camera were standardized with a calibrated target for each microscope objective. In this way, the hardness H ($H = F/A_{imprint}$) was determined with the known $\beta.F$ load applied. The visualized indent surfaces (a few square microns cf. **Fig. 11**) are nearer to a spherical indenter imprint than the one made by conical indenter. One way to determine which shape of the indenter was leading is to calculate the $h_{imprint}$ indentation contact depth from the projected area. The relationship between projected surface $A_{Imprint}$ and penetration or indentation contact depth $h_{Imprint}$ for a spherical indenter is given by:

$$A_{Imprint} = -\pi.h_{imprint}^2 + 2\pi.R.h_{imprint} \quad (5.1)$$

and for a conical indenter:

$$A_{Imprint} = \pi.h_{imprint}^2.tg^2\theta \quad (5.2)$$

For a layer of 1.4 mm thickness with $A_{imprint} = 4.5\ \mu m^2$, $\theta = 30.65°$ and R = 20 µm, from the Eq. 5.1 and Eq. 5.2 one obtains $h_{Imprint}$ = 36 nm for a spherical

indenter and $h_{Imprint}$ = 2 µm for a conical indenter. Yet, 2 µm is greater than the layer thickness, which is not possible in this case because the tip displacement was 800 nm at most. Thus, the $h_{imprint}$ obtained for a conical indenter is incompatible with the layer thickness and with the h tip displacement, which confirms the SEM photography analyze (**Fig. 4**). For the scratches, the relationship becomes:

Spherical indenter $$A_{Imprint}=2 .L.\sqrt{R^2-2.h.R+h_{imprint}^2} \quad (6)$$

where L is the length of the scratch measured experimentally on photograph taken with the microscope.

Another way to verify the accuracy of assimilating the indenter shape to a spherical shape is to calculate the $h_{imprint}/R$ ratio, where $h_{imprint}$ is 0.2 µm for its highest value (determined from the highest measure of $A_{Imprint}$ and from the Eq. 5.1). One should find $\frac{h_{imprint}}{R} \leq 1 - sin\,\theta$ [29], with θ half the angle of the indenter equal to 30.65°. This gives $h_{imprint}/R = 1.10^{-2}$. The inequality is verified. Thus, the determination of the hardness, in particular the projected area $A_{Imprint}$ was done by considering the indenter with a spherical shape.

3. Manufactured sample and results

3.1 Sol-gel layer used

The sol-gel layers were deposited by spin-coating technique with a hybrid silica-PDMS solution on a 50 mm diameter and 5 mm thickness silica polished substrate. The material synthesis is made from tetraethylorthosilicate and a PDMS reagent that leads to a silica-PDMS ormosil formulation via a sol-gel reaction [6]. The substrate is then coated with the ormosil solution. The spin coating technique [30] consists of putting a few drops of the sol-gel solution on a substrate while it is rotating at high speed. The rotation caused the solution to spread approximatively uniformly on the substrate and the thickness was controlled with the solution viscosity and the rotation speed. The spinning speeds used to make our layers were between 1,500 and 4,000 rpm and were maintained for 20 seconds, with an acceleration rate of 1,000 $rpm.s^{-1}$. The substrates were coated at room temperature. An appropriate heat treatment was carried out at 120°C during 1.5 hours with pre-heating steps (**Fig. 12**) to avoid the apparition of thermal stress inducing cracks in the coating.

This thermal treatment eliminated solvents and undesirable products obtained from the chemical reaction and still there. Moreover, it also activated the chemical bounds between the surface silanol groups (Si-OH) of the substrate and the sol-gel species of the layer to increase layer hardness. The main parametric studied concerned the variation in mass (expressed in wt. %) of PDMS (from 10 to 40 wt. %) in the polymeric silica, the pattern number n of

the PDMS chain 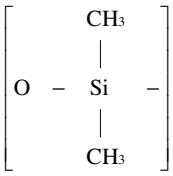 and the catalysis used during the synthesis:

either hydrochloric acid (HCl) or triflic acid (trifluoromethanesulfonic TFS). The film thickness was measured thanks to a spectrophotometer Perkin-Elmer after thermal treatment [31- 32]. Two types of PDMS were used, one with a viscosity of 0.25 St and a molar mass estimated around 550 $g.mol^{-1}$ according to the supplier Sigma-Aldrich, the other between 18 and 22 St and a molar mass measured around 14,234 $g.mol^{-1}$. The difference in viscosity is related to the difference in the length of the PDMS chain (n) that we measured by using an exclusion chromatography (see Table 1) [33].

3.2 Determination of the hardness and elastic modulus

The curves of loading versus contact depth given in **Fig. 13** show the differences in hardness of hybrid silica-PDMS layers. For a same value of load, the $h_{imprint}$ contact depth is higher for the formulations with a lesser PDMS ratio. For example, in the case of the PDMS with a molar mass of 550 $g.mol^{-1}$ and a viscosity of 0.25 St, the layer silica-PDMS at 40 wt. %, for a same value of load, has a lesser residual penetration of the tip than the one with 30 wt. % PDMS and this latter has also a lesser residual penetration than the one with 40 wt. % PDMS. Experimentally, we only have access to the value of the plastic deformation, and thus the residual tip penetration as we

determined $h_{imprint}$ from the image of the contact surface $A_{imprint}$. For small values of load (less than 35 μN), the behavior of the hybrid at 10 wt. % and 30 wt. % PDMS is similar. So, having a penetration depth lower when the ratio of PDMS increases in the hybrid silica-PDMS, for a given value of load (higher than 35 μN) is explained by the difference in elasticity of the hybrids caused by the introduction of the PDMS in the rigid polymeric silica matrix [4-5]. Indeed, for a higher value of the PDMS ratio, the material is less rigid, as the PDMS is an elastomer. Thus, the elastic response of the hybrid increases with the PDMS ratio, explaining why the residual penetration depth measured is lower with 40 wt. % PDMS. So, when the tip lowers, once positioned at the contact surface, the elasticity of the layer allows the tip to vertically displace from a certain distance before penetrating the layer and thus, damaging it. It is the surface displacement around the contact surface due to the elastic response of the layer. As we only have access to the residual penetration depth, the more $h_{imprint}$ value is high, the more the layer is rigid for a given tip displacement. Moreover, the influence of the viscosity is also visible on the **Fig. 13**. The layers with PDMS at 22 St in viscosity show a deeper penetration of the tip for a given load compared to the other layers made with the PDMS at 0.25 St. As expected, viscosity and elastic properties are two important parameters that influence the hardness of layers.

The relative hardness measurements of the various ormosil layers are given in **Fig. 14**. The trend of the hardness is to increase with the length of the

PDMS chain (the more the chain is long, the more the viscosity is high) and with TFS catalysis. Plus, the hardness decreases when the PDMS ratio increases, as seen above. However, when it comes to nano-indentation, a question remains: how to be sure that what is measured is not the hardness of the substrate? Usually, the Bückle rule provides a reasonable starting point [34]: the indentation depth should not exceed 10% of the layer thickness if you want to measure the hardness of the layer without any substrate effect. Otherwise, the plastic response associated with the indentation will be contained entirely within the film and the elastic response of the substrate will be negligible. In cases where the film is not too thin and the indenter not too blunt the assumption gives reasonable results. However, experimental and numerical studies on coated materials have shown the inadequacy of this rule [35, 36]. According to these works, although there is no elastic deformation (on the part of the substrate), the response of the film-substrate system corresponds to the film response only for indentation depths less than 1% of the thickness. In addition, for an indentation depth beyond 2% of the film thickness, the elastic response of the coated substrate differs from the film and may account from 10% to 90% in the values measured for the deposited layer. This explains why in the experiments of this article, the tip has not been pushed more than 1% of the layer thickness (**Fig. 14. a**). Even though the tip penetrated the film of less than 1%, the effects of the substrate are visible on some hardness vs penetration depth curves (**Fig. 14. a**). Indeed, on such

curves, the hardness has three areas of variation with depth of indentation: growth (at low loads), plateau and decay for large deformations [37] as shown in **Fig. 13. b**. The curves derived from our experiments (**Fig. 14. a**) follow the ones of the literature (**Fig. 14. b**). The value of the hardness on the plateau is attributed to the film [37]. Indeed, once we have a fully developed plastic zone, the hardness of the film should reach a constant or a plateau. At larger loads, or greater depths, the influence of the substrate will not be negligible and the hardness may increase or decrease according to the relative hardness of the film and substrate. As we used a tip that was not sharp enough, it is normal to see the influence of the substrate surface even at very small depth penetrations [37]. Indeed, if the indenter is too blunt, then most of the deformation may be elastic and the mean contact pressure so measured will not reflect perfectly the film hardness.

Knowing the displacement of the tip during the loading and the depth of penetration h after the unloading for the point matrix, we can determine the elastic modulus E_t of the layer by using the relationship given by Sneddon [38] and the reduced modulus E_{rsl} [39-40]:

$$E_{rsl} = \frac{1}{\gamma}\frac{\sqrt{\pi}}{2}\frac{S}{\sqrt{A(h)}} \text{ with } \frac{1}{E_{rsl}} = \frac{\left(1-\upsilon_{sl}^2\right)}{E_{sl}} + \frac{(1-\upsilon_t^2)}{E_t}$$

where: S is the contact stiffness, S = dF/dh, ν_{sl} and ν_t are the Poisson's ratio of the layer and the tip respectively, E_t is the elastic modulus of the tip, γ is a geometrical constant of the order of unity. The contact stiffness has been

calculated by determining the h_s surface displacement around the contact surface due to the elastic response of the layer. It is given by: $h = h_s + h_{imprint}$, where h is the tip displacement. The F load, even given relatively to a β coefficient (taken equal to 1 here), permits to find values of the elastic modulus very close to results coming from the commercial nano-indenter of the Anton Paar Company (**Fig. 15. a**). Differences appear between the results from the homemade nano indenter and those from the commercial indenter as the results from the homemade nano indenter are only relatives. However, the trend remains: the value of the elastic modulus is higher with a higher wt. % PDMS. Furthermore, the relative elastic modulus increases with TFS catalysis. It decreases with the PDMS ratio (**Fig. 15. a**). Thus, we find again the trends obtained by Mackenzie [11] about the PDMS mass bulk (**Fig. 15. b**).

3.3 Scratches: mechanism of self-healing

In **Fig. 16,** an evolution over time of the scratches for some layers has been observed. For example, when the PDMS (550 $g.mol^{-1}$) ratio reached 40 wt. % with HCl catalysis, a self-healing effect of the thin film is shown. Indeed, when observed with a magnification microscope of X50, the scratches decreased over time. When the PDMS ratio reached 30 wt. % with HCl catalysis, no evolution of the scratches over time is observed. Scratches at 200

nm and 500 nm depth fade clearly over time at room temperature, showing a self-repair mechanism of the layer since a large part of the damage is erased in a few hours. Having healing properties with only the 40 wt. % layer (in the case of PDMS 550 $g.mol^{-1}$) shows that the mechanism governing the repair is largely related to viscoelastic phenomena characterized by stress relaxation leading to damage recovery.

The kinetics of the surface evolution (**Fig. 17**) can be adjusted by two exponential functions that indicate two mechanisms of healing: one short-term (τ_1 is the decay time) and the other long- term (τ_2 is the decay time).

Our indentation measurements being made in a few minutes, the recorded surfaces stay close to indented surfaces.

The evolution has been studied from a mechanical point of view leading to a Burgers model.

The time-dependent viscoelastic response of the silica-PDMS film can be described by the Burgers model [41-42] (**Fig. 18**) which corresponds to an association of the Voigt-Kelvin model with the Maxwell model by adding up the deformations of the two models and by taking the same strain for the two models.

The Burgers model fit follows the experimental data. So, the scratches, observed in the **Fig. 16** decreased over time thanks to the viscoelastic effects of the thin film.

4. Conclusion

We modified our microscope to allow the evaluation of mechanical properties in relative terms of our hybrid layers such as the determination of hardness from the imprint surface and elastic modulus thanks to the indentation matrix. The pre-focalization made before the indentation permitted to correct the bad flatness of our silicon substrates. We were able to rank our materials in hardness from the imprint surface. The scratch tests highlighted that some of our layers had self-healing properties. Two different decay times have been identified and we found that the self-healing was linked to the layer viscosity. Our layers show viscoelastic properties over a long time which indicates that our measurements are correct because the time put to made measurement is short when compared to the characteristic times found.

We are going to improve our device with an increasing magnification of our microscope to get a larger imprint surface recorded. We will also change our tip; this one will be fixed on a stage carrying out nano-displacements. Moreover, the spring stiffness of the indenter system will be precisely determined. The addition of a nano-force sensor on the microscope will permit a better determination of the values of the mechanical properties of our hybrid layers, instead of having only a trend.

Another study will also be made to determine the viscosity of the solution silica-PDMS once deposited onto its layer form. Indeed, the viscosity of a

liquid is not the same as the viscosity of a layer. Thus, the Burgers model will be more accurate.

Finally, the optimized layer with the smallest value of hardness is the hybrid silica-PDMS with 40 wt. % PDMS.

Acknowledgments

The authors would like to thank Mr. A. Benedetto of Saint-Gobain Research Paris for his relevant comments.

References

1. W. C. Oliver and G. M. Pharr, Measurement of hardness and elastic modulus by instrumented indentation: Advances in understanding and refinements to methodology, J. Mater. Res. 19 (1) (2004) 3-20.
2. W. C. Oliver and G. M. Pharr, An Improved Technique for Determining Hardness and Elastic-Modulus Using Load and Displacement Sensing Indentation Experiments, J. Mater. Res. 7 (6) (1992) 1564-1583.
3. J. Yu, X. Xiang, S. He, X. Yuan, W. Zheng, H. Lü and X. Zu, Laser-Induced Damage Initiation and Growth of Optical Materials, Adv. Cond. Matter. Phys. (2014) 364627.
4. H. Sugiura, K. Kondo, A. Sawaoka, Dynamic response of fused quartz in the permanent densification region, J. Appl. Phys. 52 (1981) 3375-3382.
5. A. Ayouch, X. Dieudonné, G. Vaudel, H. Piombini, K. Vallé, V. Gusev, P. Belleville and P. Ruello, Elasticity of an Assembly of Disordered Nanoparticles Interacting via Either van der Waals-Bonded or Covalent-Bonded Coating Layers, ACS Nano. 6 (12) (2012) 10614-10621.
6. F. Compoint, D. Fall, H. Piombini, Ph Belleville, Y. Montouillout, M. Duquennoy, M. Ouaftouh, F. Jenot, B. Piwakowski and C. Sanchez, Sol–gel-processed hybrid silica-PDMS layers for the optics of high-power laser flux systems, J Mater Sci 51(11) (2016) 5031-5045.
7. J. H. Harreld, M. S. Wong, P. K. Hansma, D. E. Morse, G. D. Stucky, Self-healing organosiloxane materials containing reversible and energy-dispersive crosslinking domains, US patent 2004007792 A1 (2004).
8. J.H. Harreld, M.S. Wong, P.K. Hansma, D.E. Morse, G.D. Stucky, Self-healing organosilixane materials containing reversible and energy-dispersive crosslinking domains, US patent, US 6 783 709 B2 (2004).
9. O. Colombani, C. Barioz, L. Bouteiller, C. Chanéac, L. Fompérie, F. Lortie, H. Montès, Attempt toward 1D cross-linked thermoplastic Elastomers: Structure and Machanical porperties of a new sysem, Macromolecules 38 (2005) 1752.
10. O. Colombani, L. Bouteiller, Selective synthesis of non-symmetrical bis-ureas and their self- assembly, New J. Chem. 28 (2004) 1373.

11. J. D. Mackenzie, Y. J. Chung, Y. Hu, Rubbery Ormosils and their Applications, J. Non-Cryst. Solids 147 (148) (1992) 271-279.
12. J. D. Mackenzie, Q. Huang, T. Iwamoto, Mechanical properties of ormosils, J. Sol-Gel Sci. and Tech. 7 (3) (1996) 151-161.
13. H. Huang, B. Orler, G. L. Wilkes, Ceramers: Hybrid Materials Incorporating Polymeric/Oligomeric Species with Inorganic Glasses by a Sol-Gel Process, Polym. Bull. 14 (6) (1985) 557-564.
14. H. H. Huang, B. Orler and G. L. Wilkes, Structure-Property Behavior of New Hybrid Materials Incorporating Oligomeric Species into Sol-Gel Glasses. 3. Effect of Acid Content, Tetraethoxysilane Content, and Molecular Weight of Poly(dimethylsiloxane), Macromolecules 20 (6) (1987) 1322-1330.
15. H. H. Huang, G. L. Wilkes and J. G. Carlson, Structure-Property Behaviour of Hybrid Materials Incorporating Tetraethoxysilane with Multifunctional Poly(tetramethylene oxide), Polymer 30 (11) (1989) 2001-2012.
16. J. E. Mark and C. C. Sun, Polymer-modified silica glasses I. Control of sample hardness, Polym. Bull. 18 (3) (1987) 259-264.
17. P. Voarino, S. Petitrenaud, H. Piombini, F. Sabary, D. Marteau, High-precision measurements of reflectance, Proc. SPIE 6342 (2006) 540-549.
18. H. Piombini, P. Voarino, Apparatus designed for very accurate measurement of the optical reflection, Appl. Opt. 46 (36) (2007) 8609-8618.
19. H. Piombini, D. Soler, P. Voarino, New device to measure the reflectivity on steeply curved surface, Proc. SPIE 7018, doi: 10.1117/12.802192 (2008).
20. H. Piombini, X. Dieudonne, T. Wood and F. Flory, Guided wave measurements for characterization of sol-gel layers, Opt. Rev. 20 (5) (2013) 426–432.
21. H. Piombini, F. Compoint, C. Ambard, D. Picart, P. Belleville, G. Damamme and F. Brémand, Stress measurement of elastic sol-gel layer by photoelasticimetry - comparison with Stoney, Opt. Mater. Express 6 (2) (2015) 469-485.
22. D. Fall, F. Compoint, M. Duquennoy, H. Piombini, M. Ouaftouh, F. Jenot, B. Piwakowski, P. Belleville, and C. Ambard, Surface acoustic wave characterization of optical sol-gel thin layers, Ultrasonics 68 (2016) 102-107.
23. O.S. Heavens, Some factors influencing the adhesion of films produced by vacuum evaporation, J. Phys. Radium 11 (7) (1950) 355-360.
24. P. Benjamin and C. Weaver, Measurement of adhesion of thin films, Proc. R. Soc. London 254 (1960) 163-176.
25. M. Laugier, The development of the scratch test technique for the determination of the adhesion of coatings, Thin Solid Films 76 (3) (1981) 289-294.
26. J. Avice, C. Boscher, P. Voarino, G. Brotons, and H. Piombini, Quantitative estimation of crazing in sol-gel layers by automated optical microscopy analysis, Optics Express 25 (23) (2017) 28851-28869.
27. Michelle L. Oyen, Handbook of Nanoindentation: With Biological Applications, Pan Stanford, 2010, pp. 23-30.
28. C. A. Schneider, W. S. Rasband, K. W. Eliceiri, "NIH Image to ImageJ: 25 years of image analysis", Nature methods 9 (7), PMID 22930834 (2012) 671-675.
29. W. Chen, M. Li, T. Zhang, Y. Cheng, C. Cheng, Influence of indenter tip roundness on hardness behavior in nanoindentation, Materials Science and Engineering 445-446 (2007) 323-327.
30. D. P. Birnie III, Spin coating technique, Sol-gel Technologies for glasses producers and users, Springer US, New York, 2004, pp. 49-55.
31. J. Avice, C. Boscher, G. Vaudel, G. Brotons, V. Juvé, M. Edely, C. Méthivier, V. E. Gusev, P. Belleville, H. Piombini, and P. Ruello, Controlling the Nanocontact Nature and the Mechanical Properties of a Silica Nanoparticle Assembly, J. Phys. Chem. C 121 (42) (2017) 23769–23776.

32. J. Mouchart, G. Lagier, B. Pointu, Détermination des Constantes Optiques n et k de Matériaux Faiblement Absorbants, Appl. Opt. 24 (1985) 1808-181.
33. D.J. Pietrzyk, C.W. Frank, Separations: Introduction to Chromatography, Chapter 22 in: Analytical Chemistry, Academic Press, New York, 1979, pp. 476-499.
34. J. H. Westbrook, Hans Conrad, The science of hardness testing and its applications, American Society for Metals, Metals Park, OH, 1973, p. 453.
35. R. Kouitat-Njiwa, J. Von Stebut, Boundary element numerical analysis of elastic indentation of a sphere into a bi-layer material, International Journal of Mechanical Sciences 45 (2003) 317-324.
36. F. Cleymand, O. Fery, R. Kouitat, A. Billard, J. Von Stebut, Surface and Coatings Technology 200 (2005) 890-893.
37. A. C. Fischer-Cripps, Critical review of analysis and interpretation of nanoindentation data, Surface and Coating Technology 200 (2006) 4153-4165.
38. I.N. Sneddon, The relation between load and penetration in the axisymmetric boussinesq problem for a punch of arbitrary profile, International Journal of Engineering Science 3 (1) (1965) 47-57.
39. O. Maciejak, P. Aubert, Mesure de dureté par nano-indentation, Techniques de l'ingénieur NM7 200 (2007).
40. J.L. Hay, G.M. Pharr, Instrumented indentation testing, ASM Handbook 8 (2000) 231–242.
41. J. Lemaitre, J.L. Chaboche, Mécanique des matériaux solides, Dunod, France, 1988.
42. J. J. Skrzypek, A. W. Ganczarski, (Eds) Mechanics of Anisotropic Materials, Springer International Publishing Switzerland (2015).

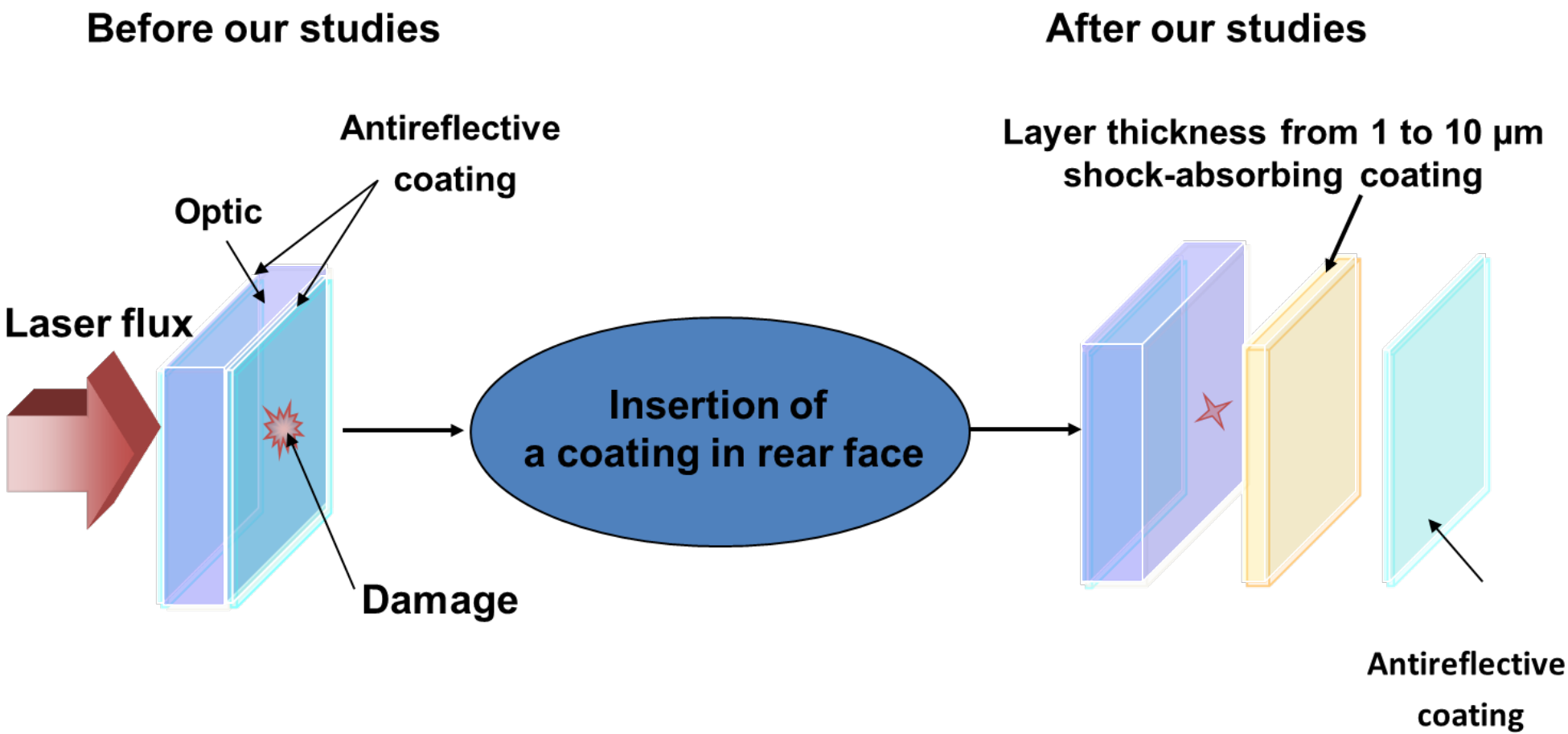
Before our studies
After our studies
Antireflective
coating
Optic
Laser flux
Damage
Insertion of
a coating in rear face
Layer thickness from 1 to 10 µm
shock-absorbing coating
Antireflective
coating

Microscope

Indenter holder

(a)

X&Y motorized stages

(b)

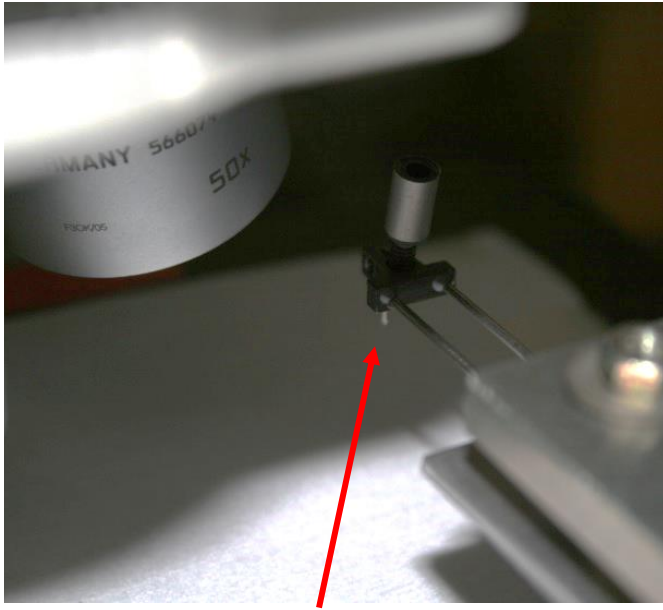

Tip with its holder

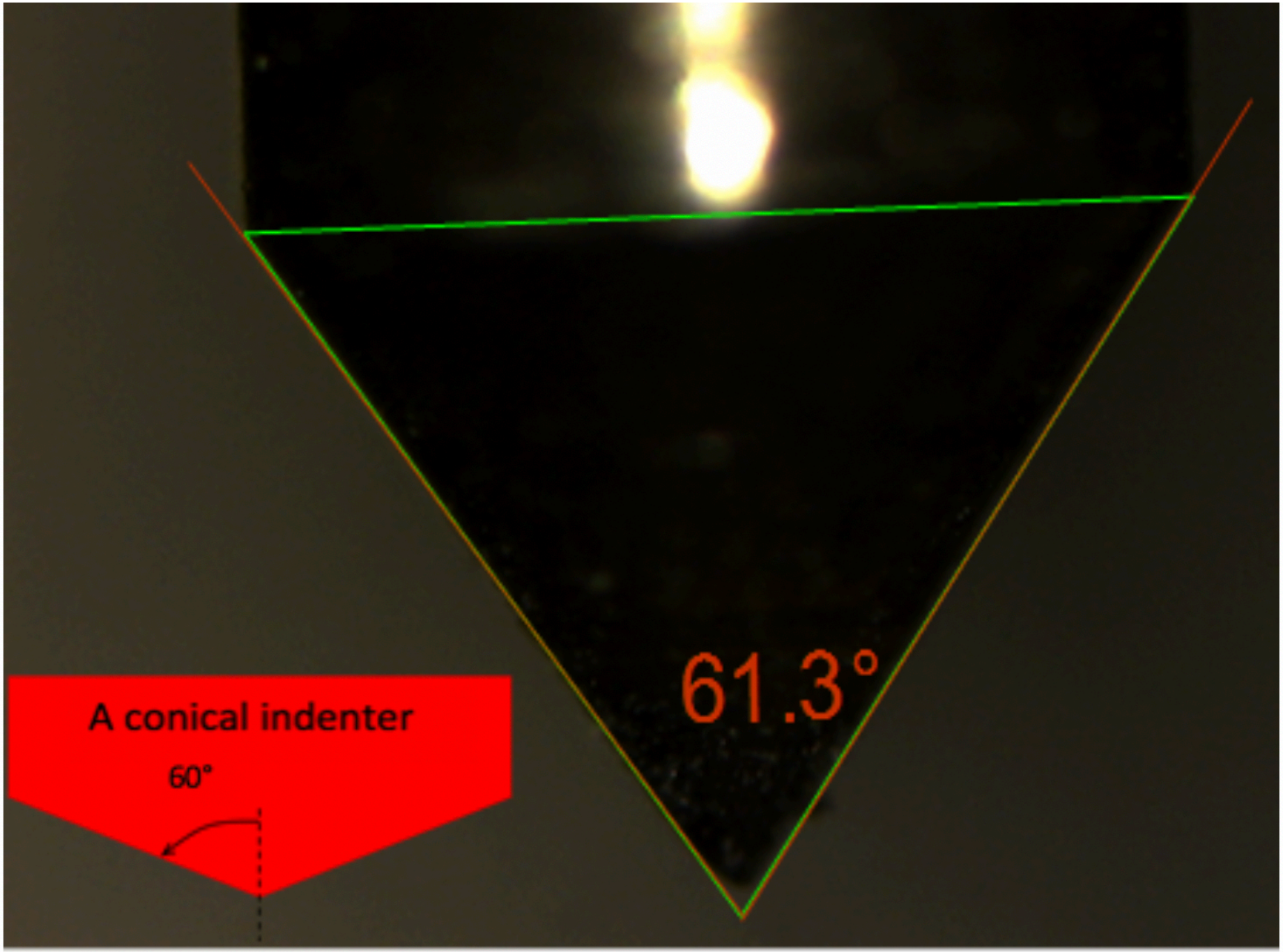
61.3°
A conical indenter
60°

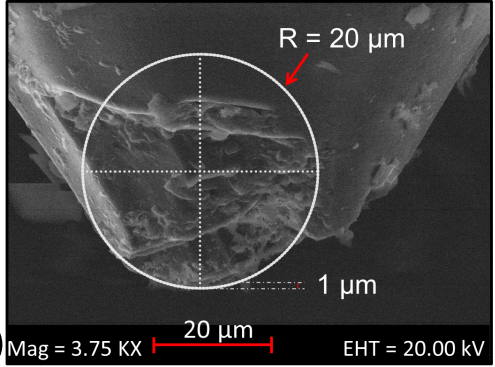

(a)

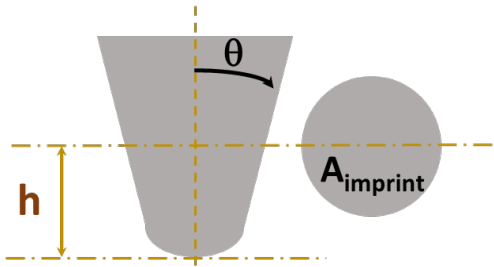

(b)

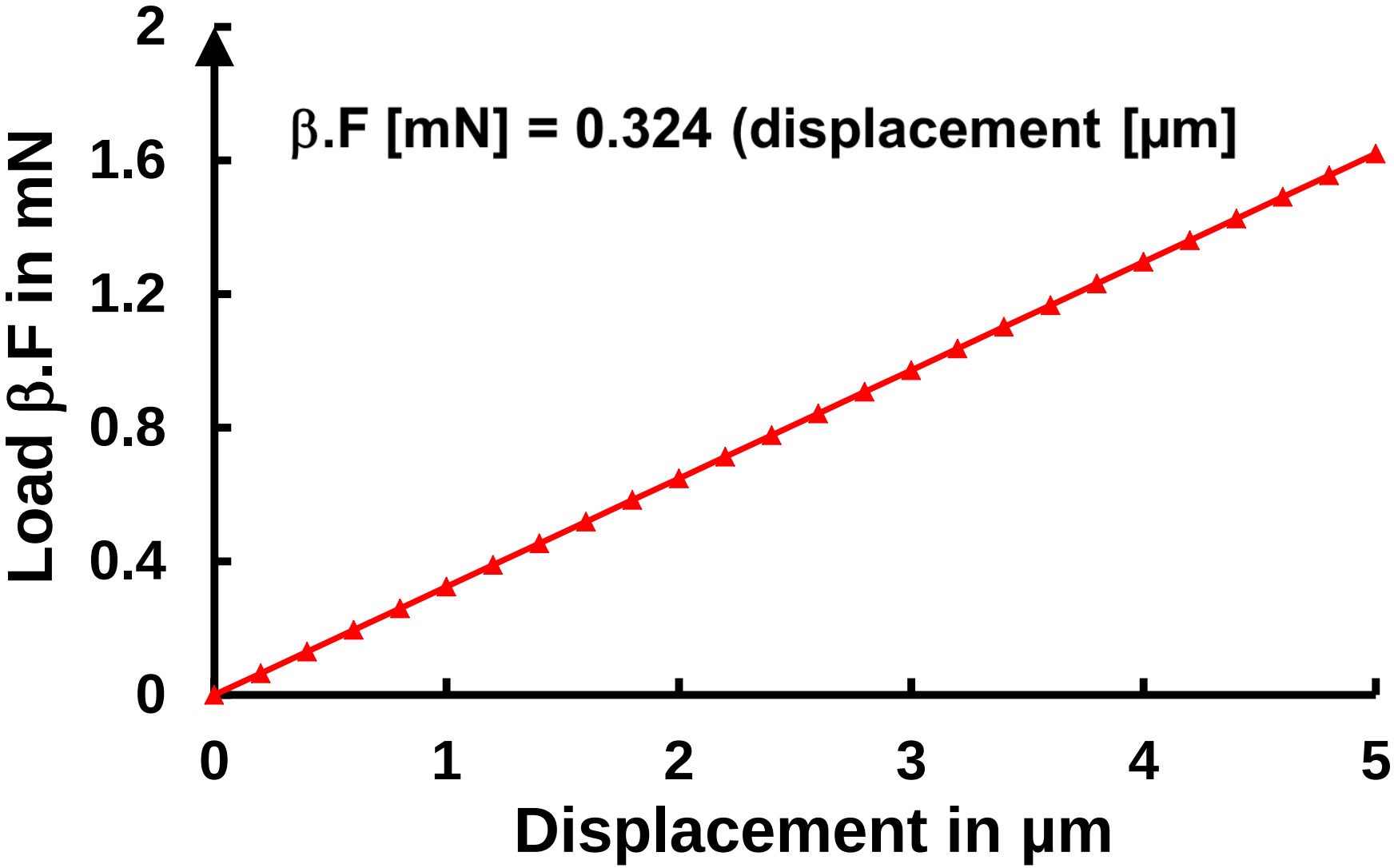
β.F [mN] = 0.324 (displacement [µm]
Load β.F in mN
2
1.6
1.2
0.8
0.4
0
0
1
2
3
4
5
Displacement in µm

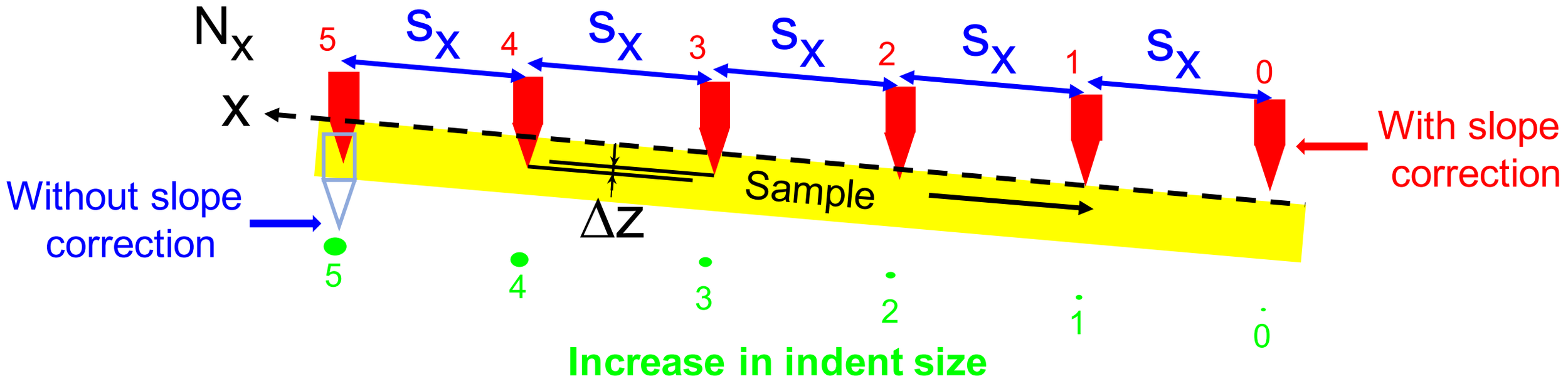
N_X
X
5
S_X
4
S_X
3
S_X
2
S_X
1
S_X
0
With slope correction
Without slope correction
Sample
Δz
5
4
3
2
1
0
Increase in indent size

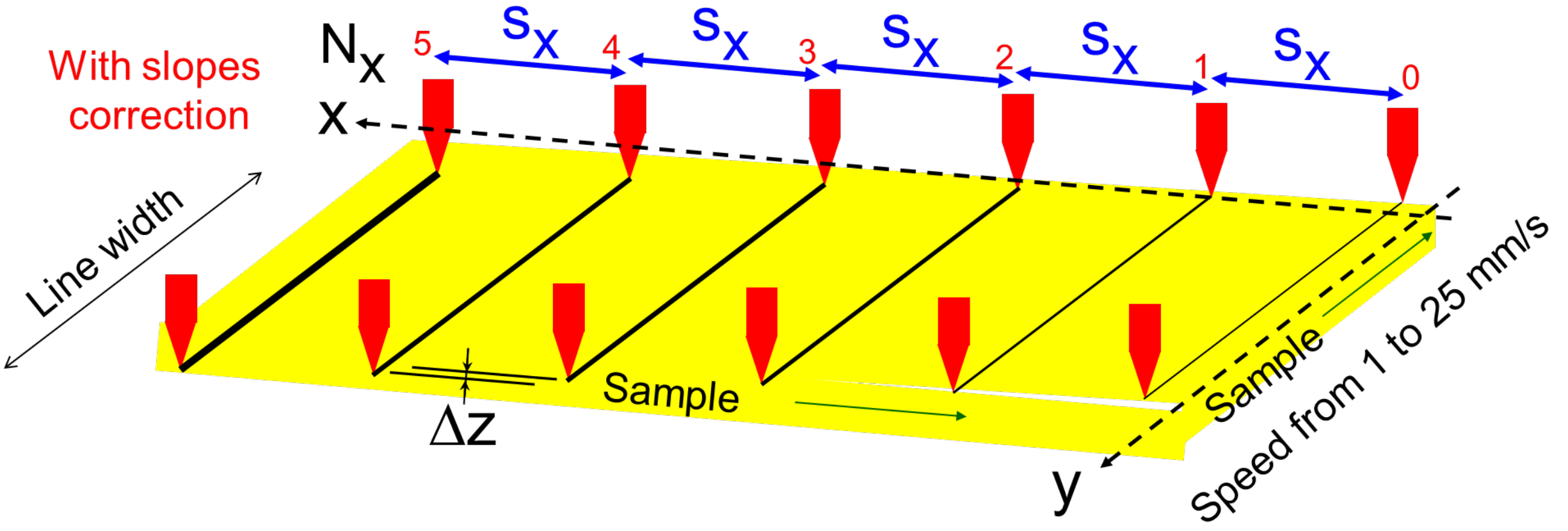
With slopes correction
N_x
x
5
4
3
2
1
0
S_X
S_X
S_X
S_X
S_X
Line width
Δz
Sample
Sample
y
Speed from 1 to 25 mm/s

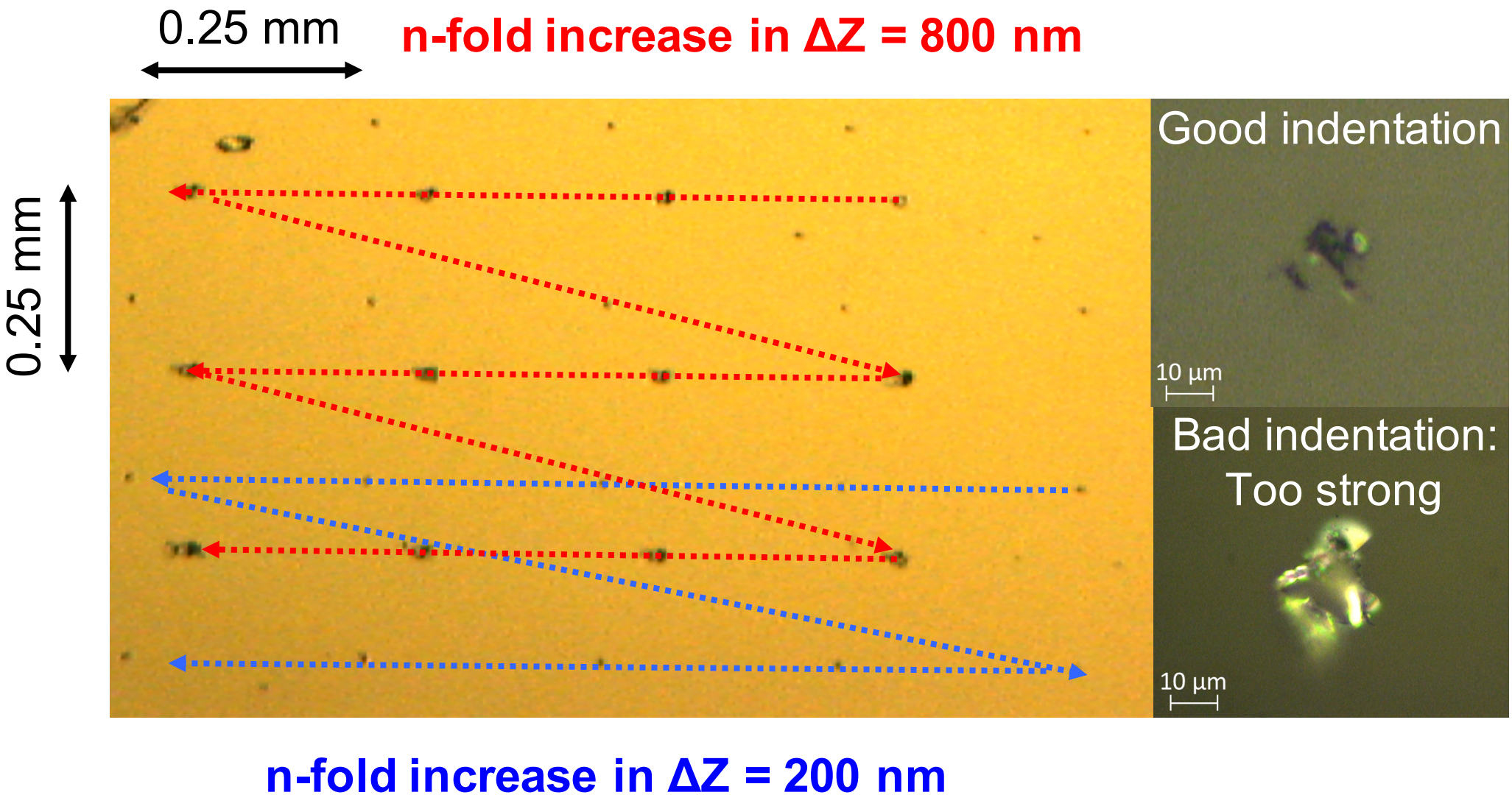
0.25 mm
n-fold increase in ΔZ = 800 nm
0.25 mm
Good indentation
10 µm
Bad indentation:
Too strong
10 µm
n-fold increase in ΔZ = 200 nm

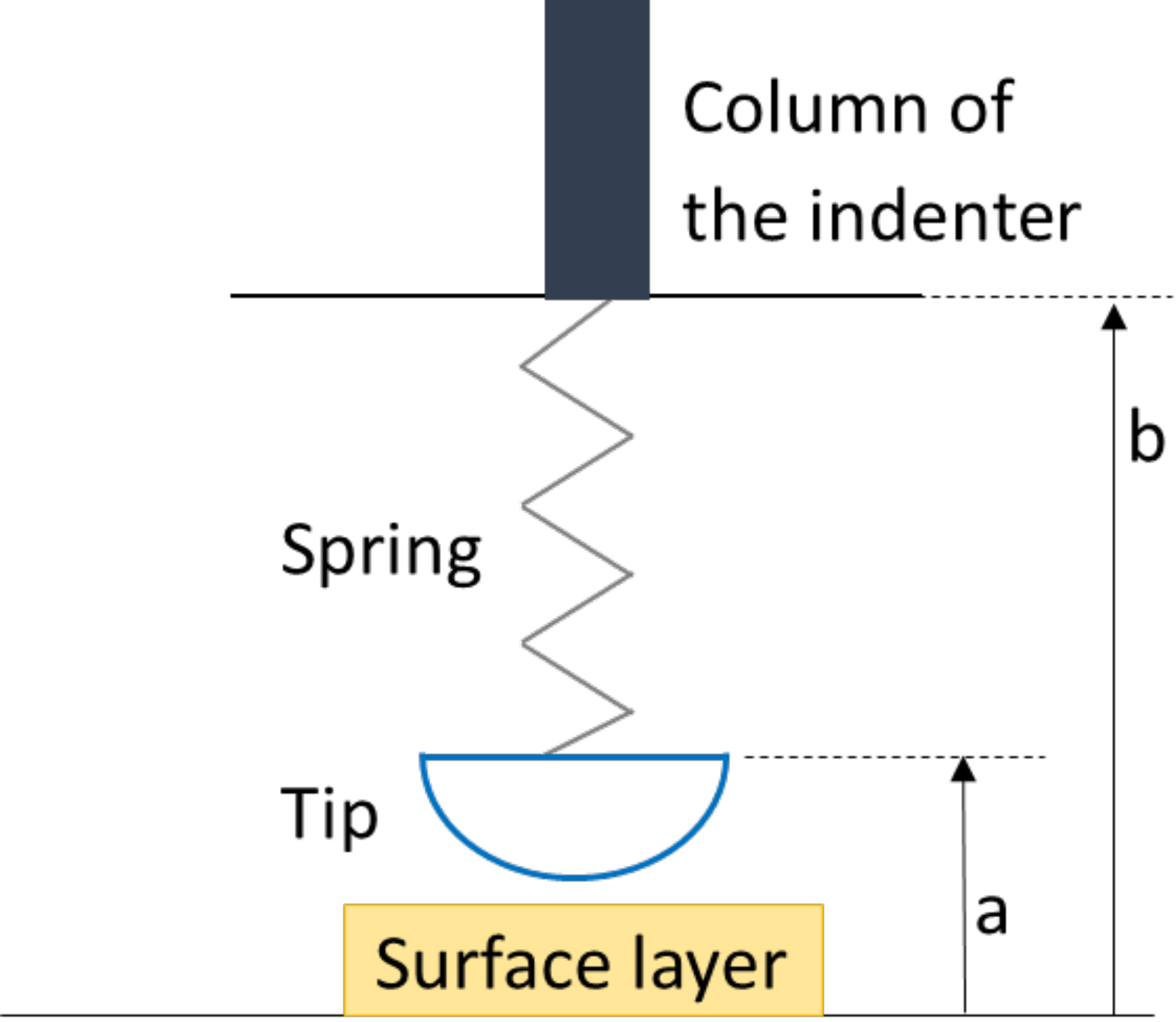
Column of
the indenter
b
Spring
Tip
a
Surface layer

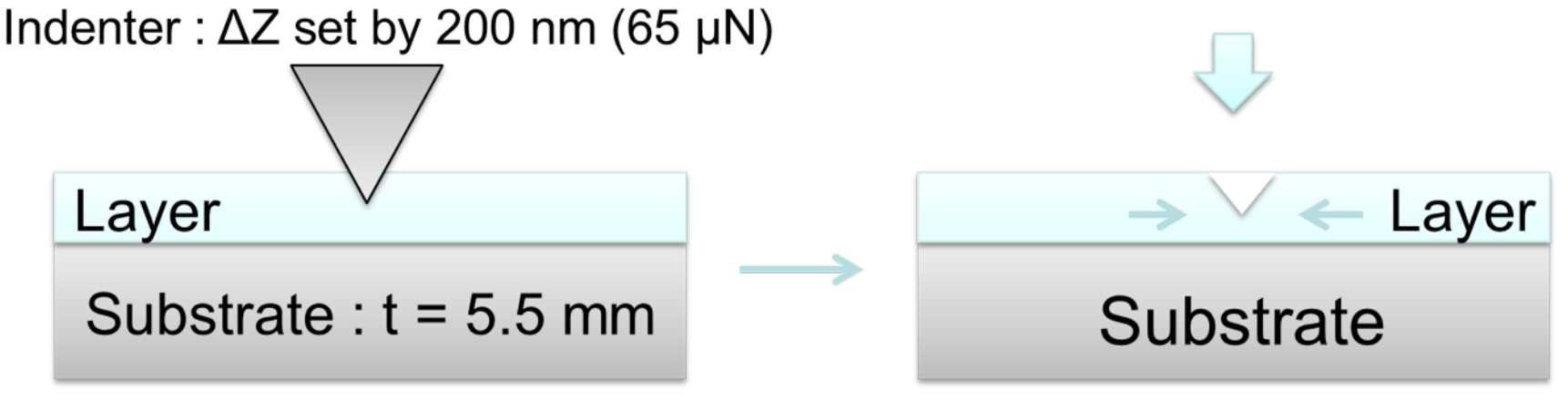
Indenter : ΔZ set by 200 nm (65 μN)
Layer
Substrate : t = 5.5 mm
Layer
Substrate

(a)

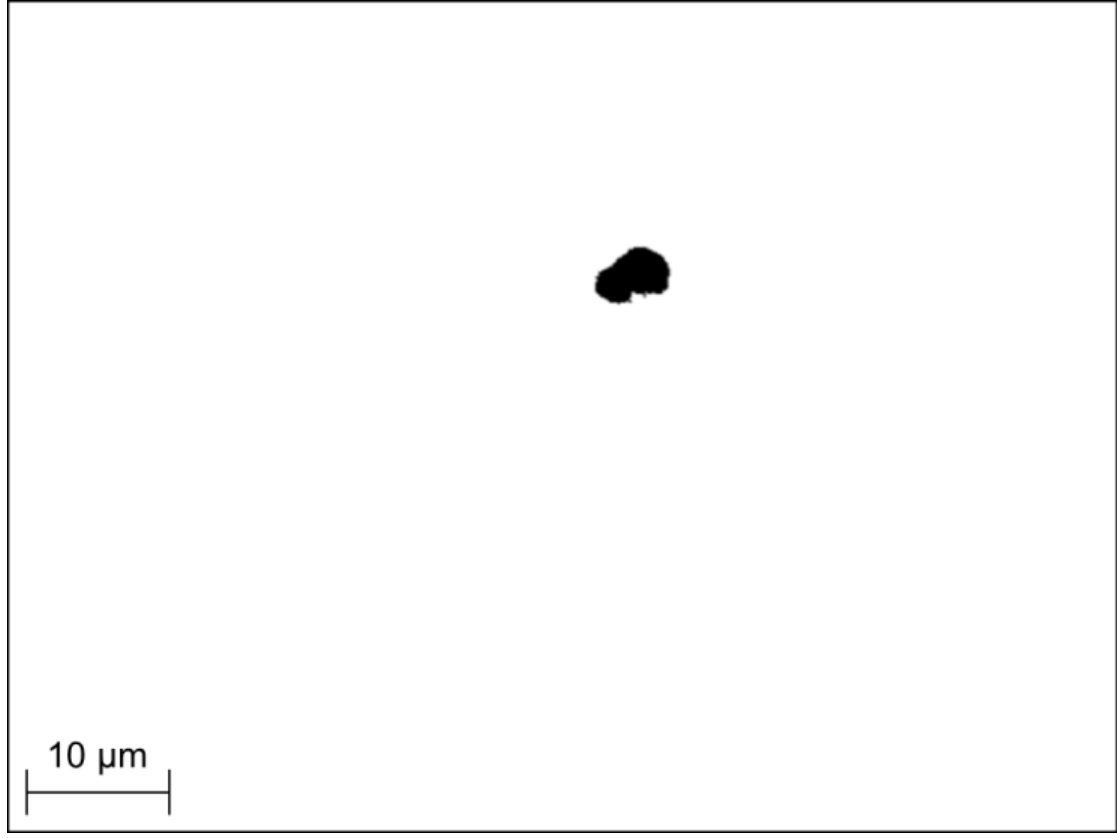

(b) Indent size A = 2.7 µm²

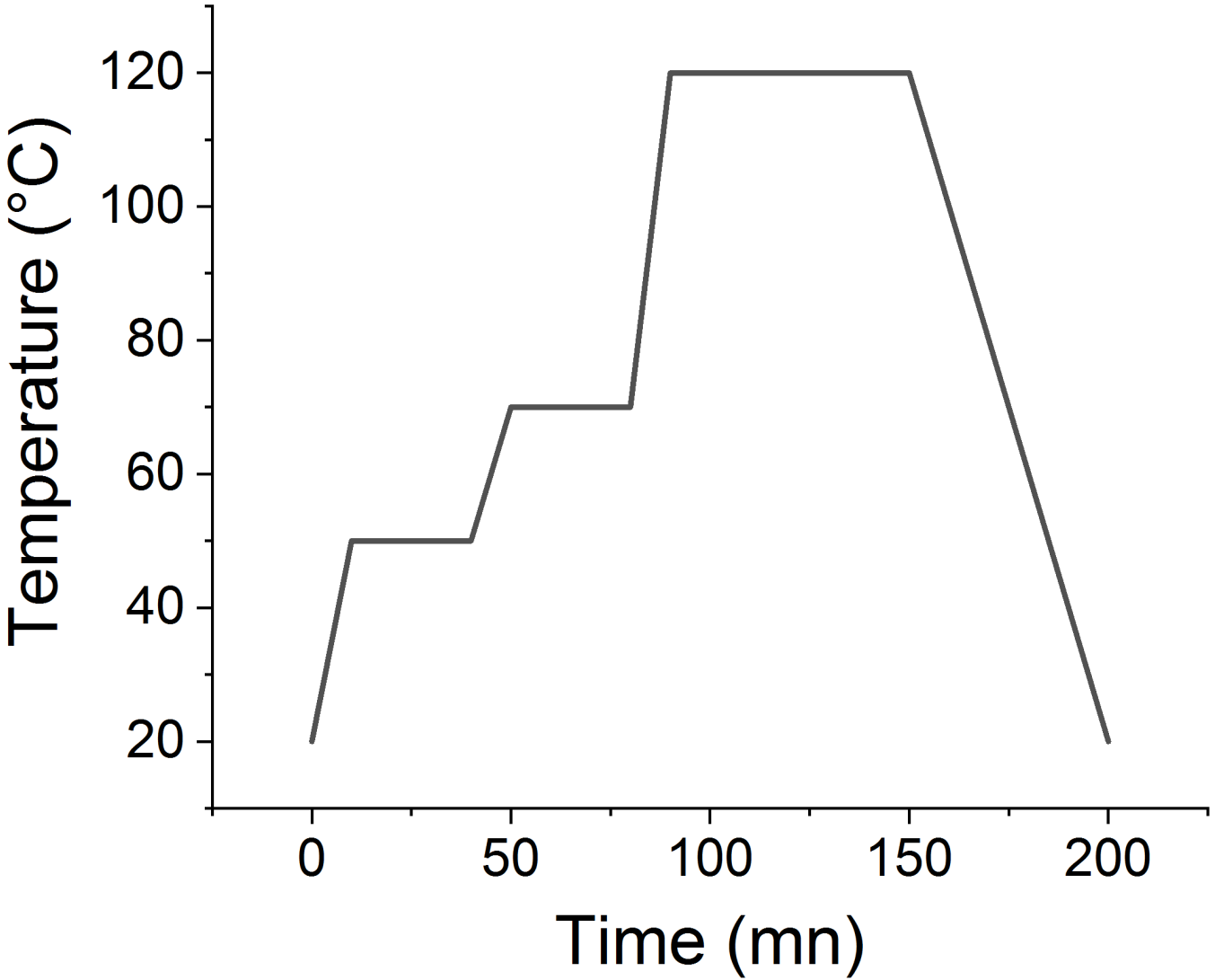
Temperature (°C)
120
100
80
60
40
20
0
50
100
150
200
Time (mn)

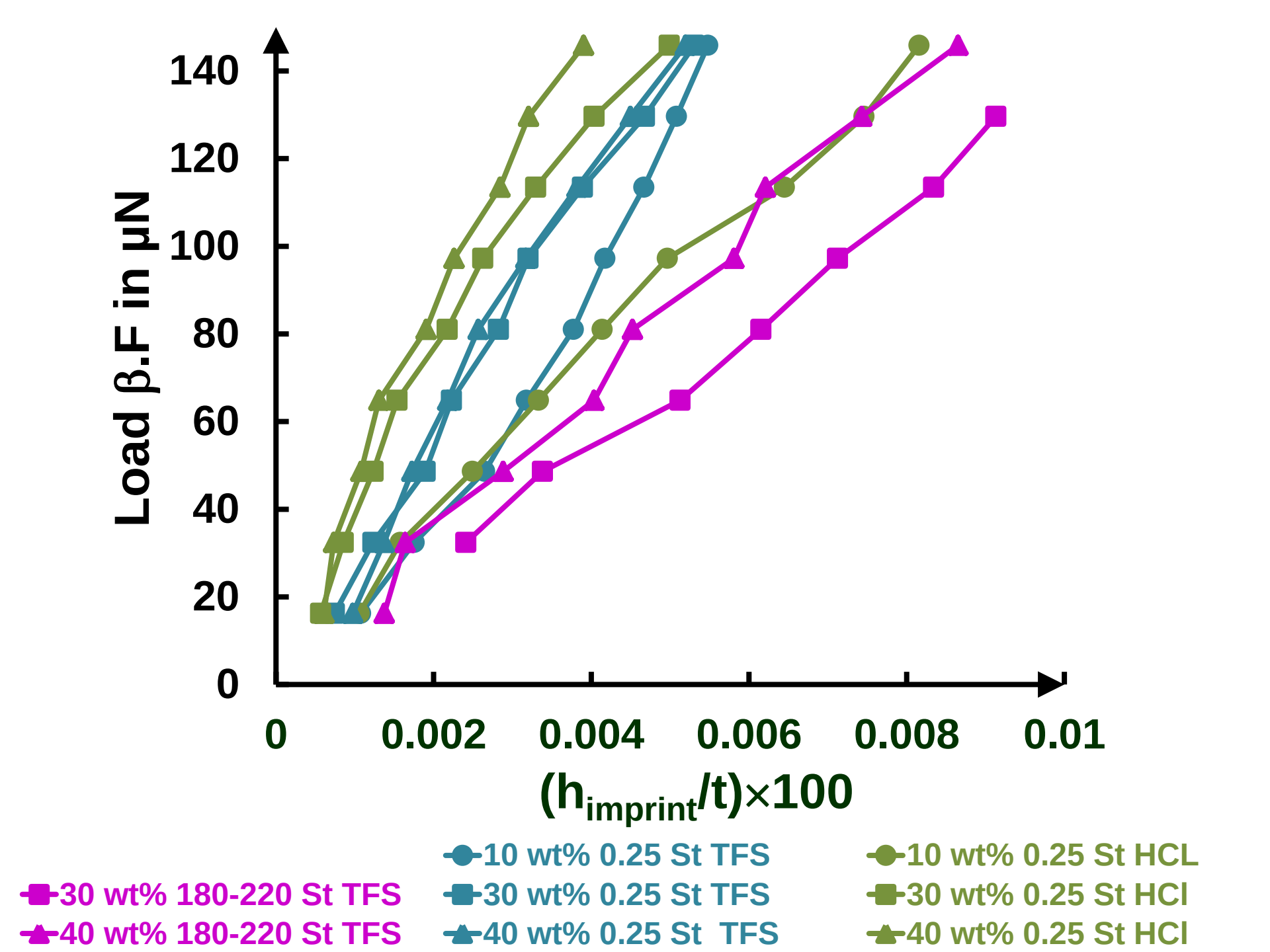
Load β.F in µN
140
120
100
80
60
40
20
0
0
0.002
0.004
0.006
0.008
0.01
(h_imprint/t)×100
10 wt% 0.25 St TFS
10 wt% 0.25 St HCL
30 wt% 180-220 St TFS
30 wt% 0.25 St TFS
30 wt% 0.25 St HCl
40 wt% 180-220 St TFS
40 wt% 0.25 St TFS
40 wt% 0.25 St HCl

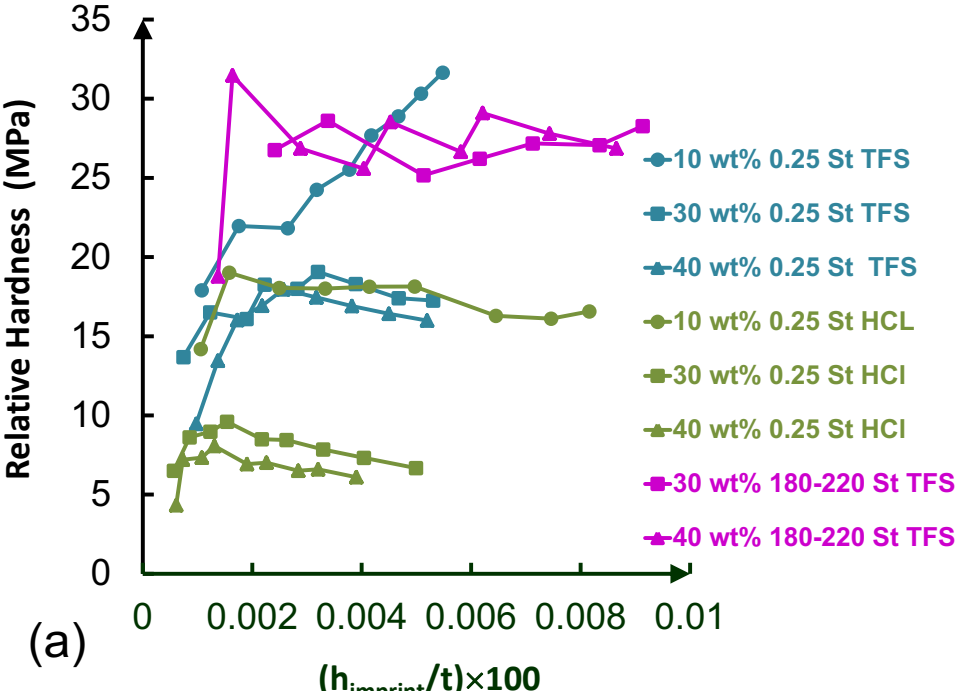
Relative Hardness (MPa)
35
30
25
20
15
10
5
0
0
0.002
0.004
0.006
0.008
0.01
(h_imprint/t)×100
10 wt% 0.25 St TFS
30 wt% 0.25 St TFS
40 wt% 0.25 St TFS
10 wt% 0.25 St HCL
30 wt% 0.25 St HCl
40 wt% 0.25 St HCl
30 wt% 180-220 St TFS
40 wt% 180-220 St TFS
(a)

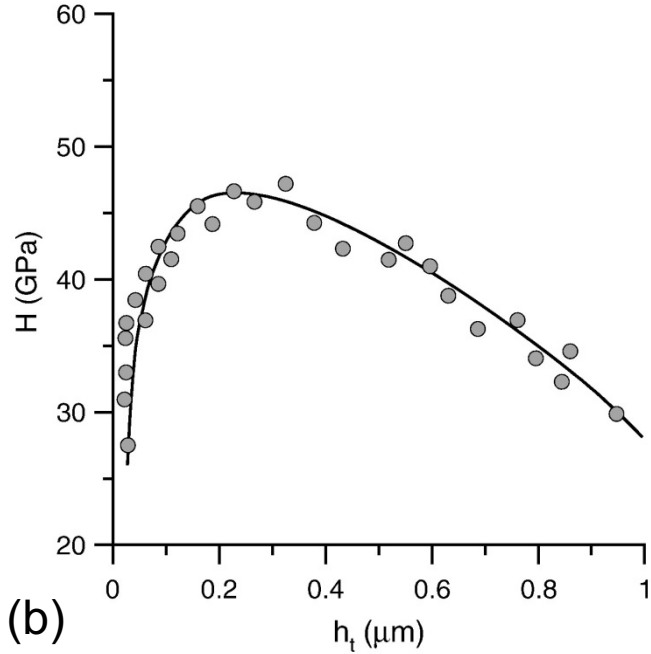
H (GPa)
60
50
40
30
20
0
0.2
0.4
0.6
0.8
1
h_t (μm)
(b)

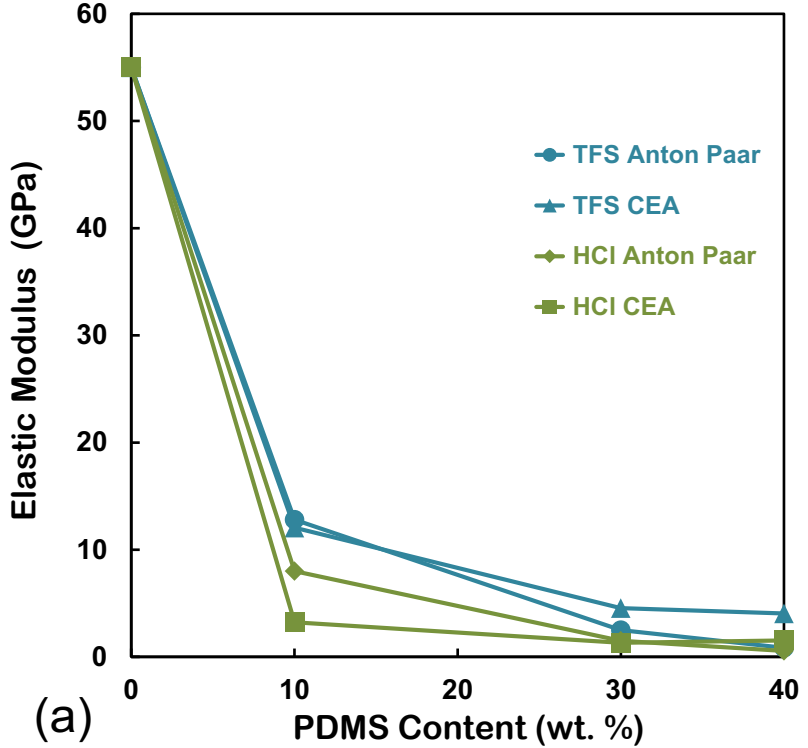
Elastic Modulus (GPa)
PDMS Content (wt. %)
TFS Anton Paar
TFS CEA
HCl Anton Paar
HCl CEA
(a)

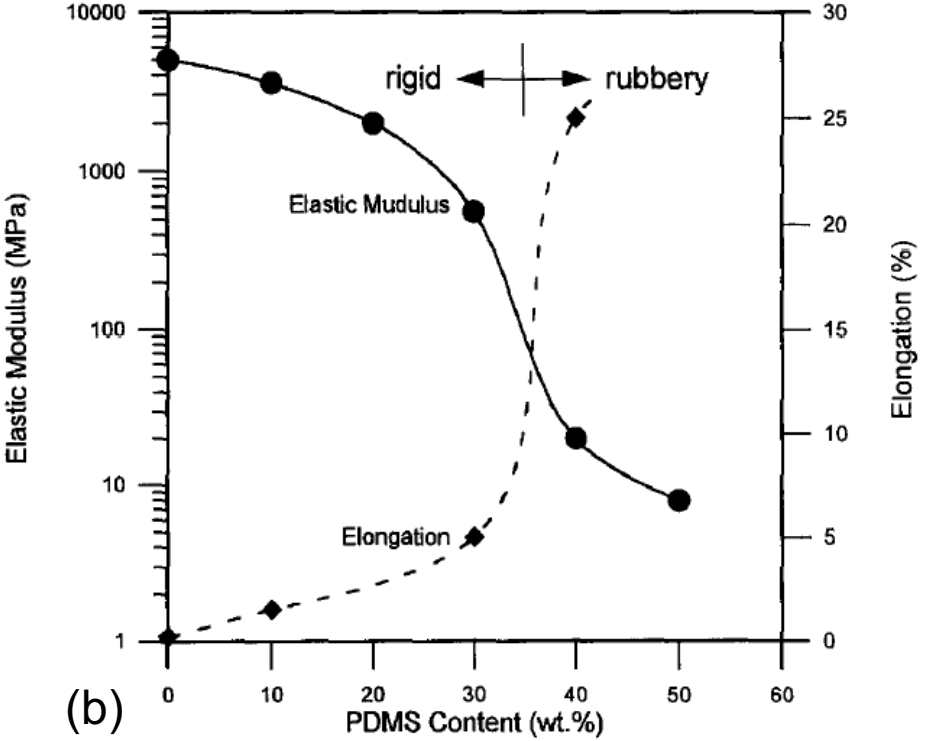
Elastic Modulus (MPa)
Elongation (%)
PDMS Content (wt.%)
rigid
rubbery
Elastic Mudulus
Elongation
(b)

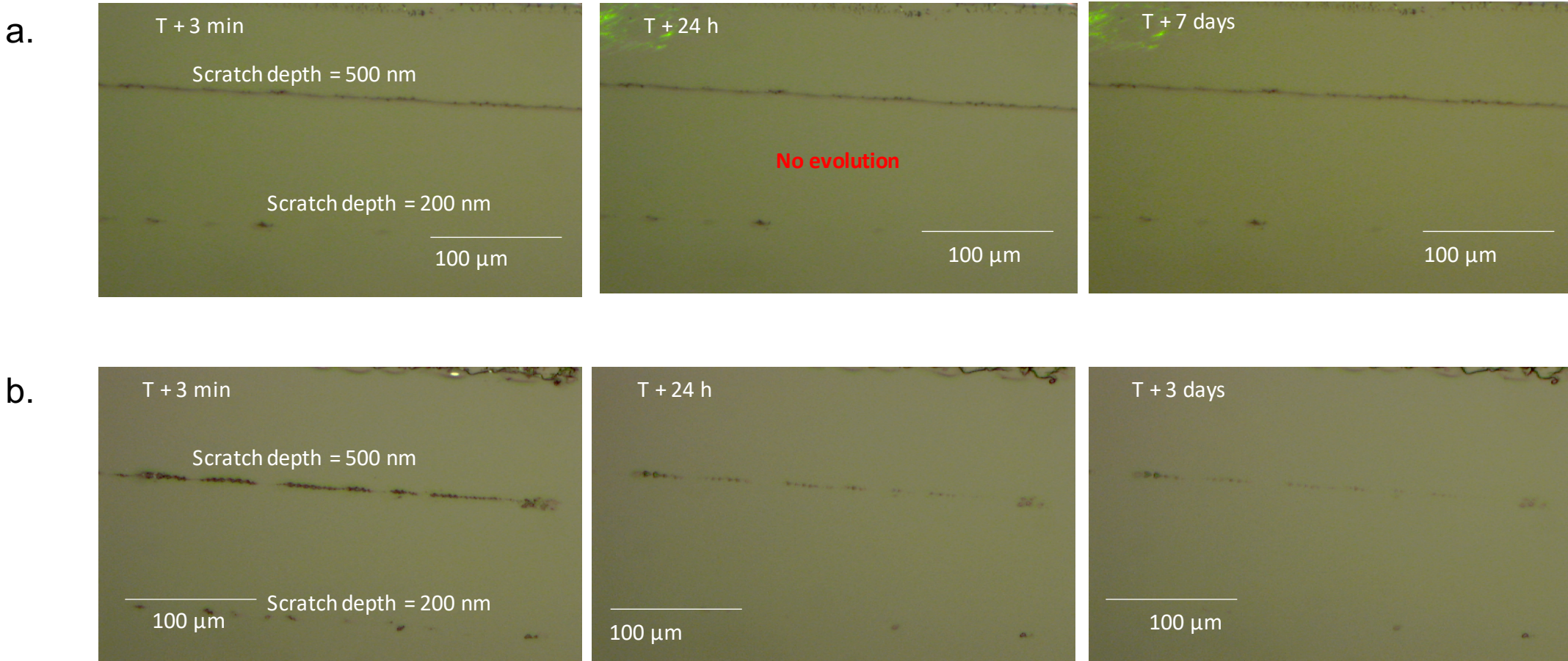
a.
T + 3 min
Scratch depth = 500 nm
Scratch depth = 200 nm
100 µm
T + 24 h
No evolution
100 µm
T + 7 days
100 µm
b.
T + 3 min
Scratch depth = 500 nm
100 µm
Scratch depth = 200 nm
T + 24 h
100 µm
T + 3 days
100 µm

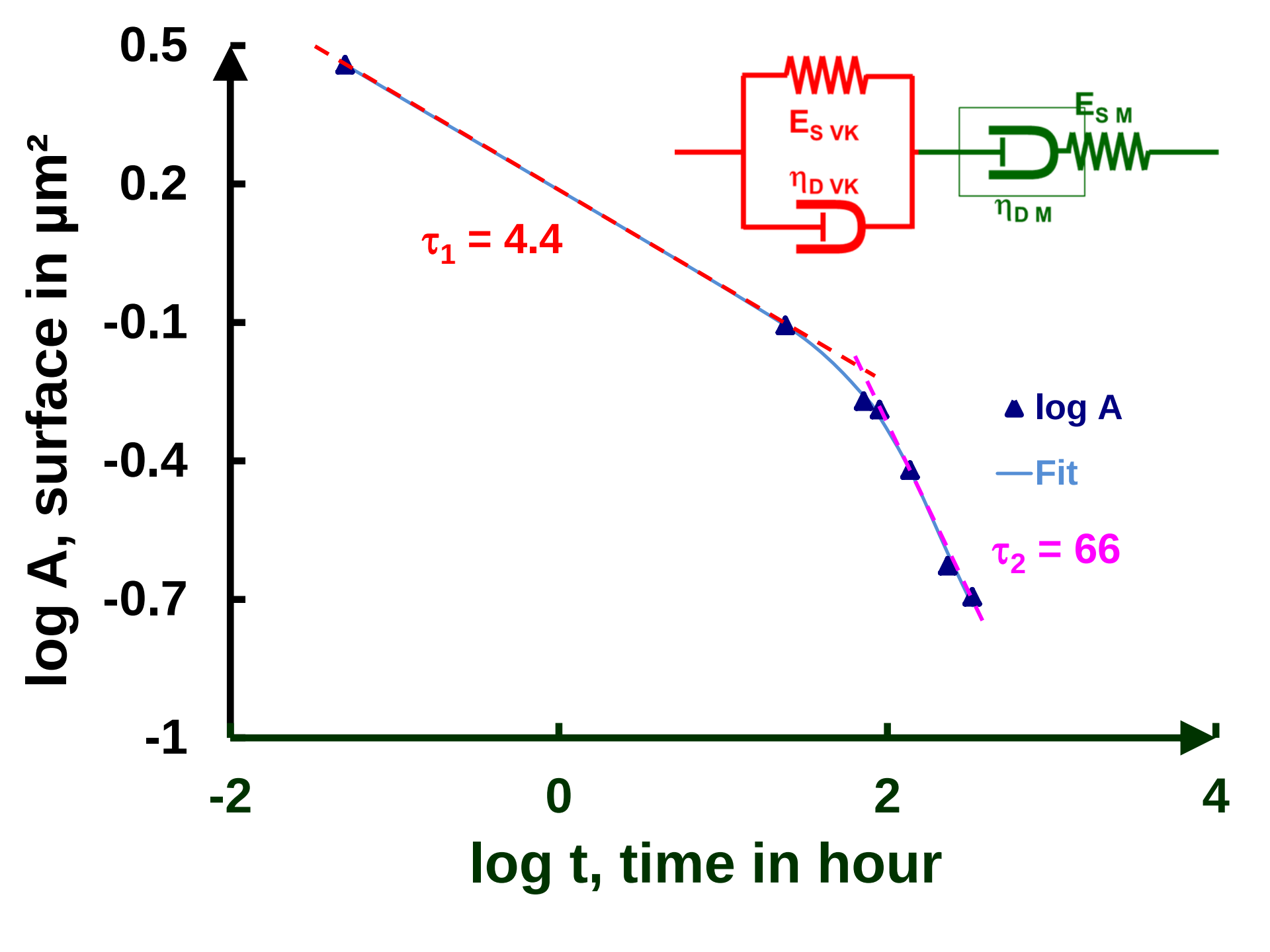
0.5
0.2
-0.1
-0.4
-0.7
-1
log A, surface in µm²
-2
0
2
4
log t, time in hour
τ1 = 4.4
τ2 = 66
log A
Fit
ES VK
ηD VK
ES M
ηD M

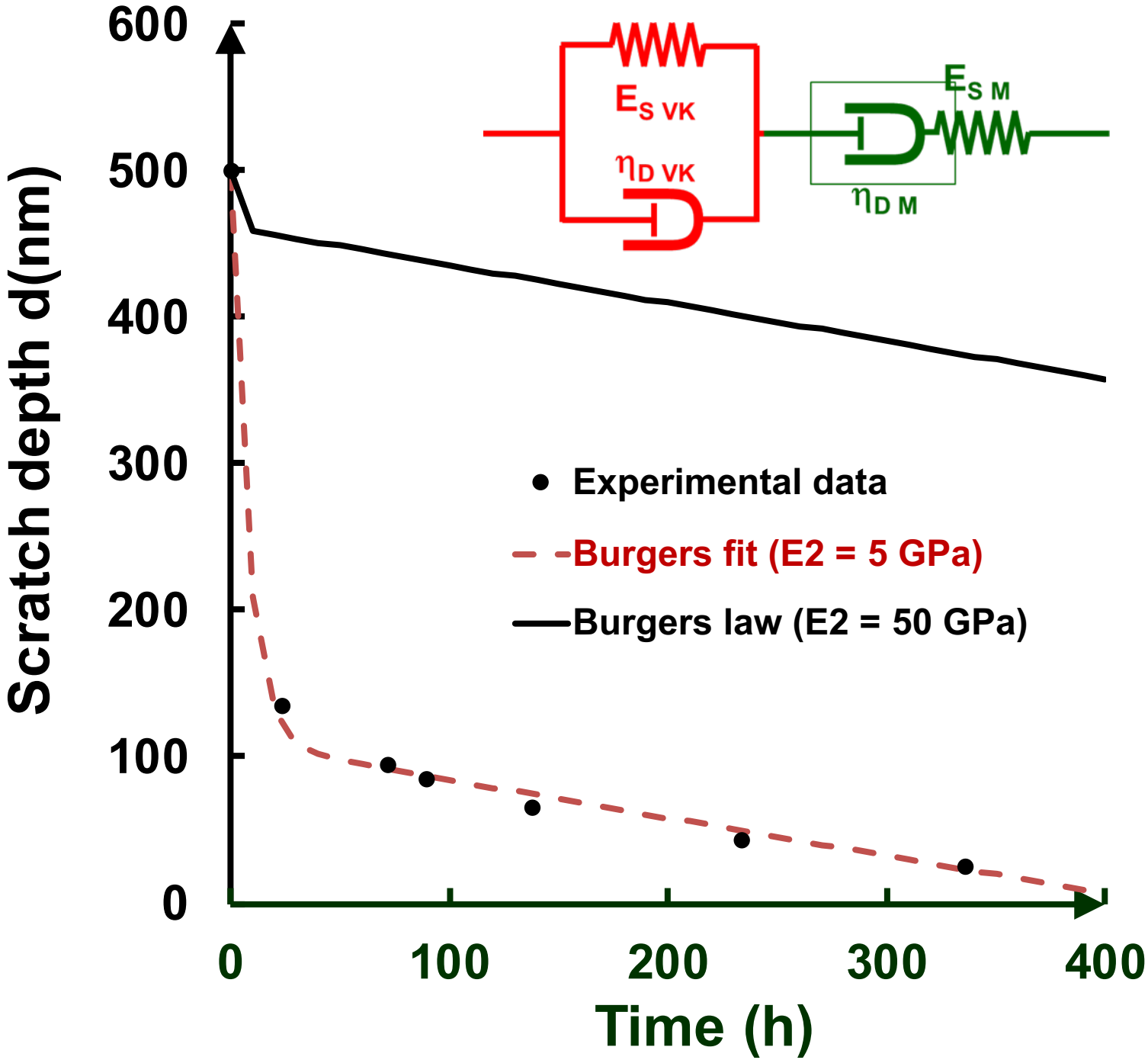
600
500
400
300
200
100
0
Scratch depth d(nm)
0
100
200
300
400
Time (h)
$E_{S\ VK}$
$\eta_{D\ VK}$
$E_{S\ M}$
$\eta_{D\ M}$
Experimental data
Burgers fit (E2 = 5 GPa)
Burgers law (E2 = 50 GPa)

Commercial Viscosity (St)	Commercial molar mass ($g.mol^{-1}$)	Molar mass ($g.mol^{-1}$)	Pattern number of the PDMS chain (n)
0.25	550	686	9
18 – 22	/	14,234	192